

J Mater Sci (2010) 45:2696–2702
DOI 10.1007/s10853-010-4254-5

Photocatalytic reduction of methylene blue by TiO₂ nanotube arrays: effects of TiO₂ crystalline phase

Xiongwu Kang · Shaowei Chen

Received: 13 October 2009 / Accepted: 20 January 2010 / Published online: 4 February 2010
© The Author(s) 2010. This article is published with open access at Springerlink.com

Abstract TiO₂ nanotube arrays were synthesized by anodization of Ti metal sheets followed by thermal annealing at elevated temperatures from 400 to 600 °C. Scanning electron microscopic measurements showed that dense arrays of nanotubes were produced with the inner diameter about 100 nm, wall thickness 35 nm, and length about 10 μm. X-ray diffraction measurements showed that the as-prepared nanotubes were largely amorphous, whereas thermal annealing led to the formation of well-defined anatase crystalline phase. More interestingly, at 470 °C, the brookite crystalline phase also started to emerge, which became better defined at 500 °C and disappeared eventually at higher temperatures, a phenomenon that has not been observed previously in TiO₂ nanotube arrays prepared by anodization. The impacts of the TiO₂ nanocrystalline structure on the photocatalytic activity were then examined by using the reduction of methylene blue in water as an illustrating example. Upon exposure to UV lights, the visible absorption profiles of methylene blue exhibited apparent diminishment. Based on these spectrophotometric measurements, the corresponding pseudo-first-order rate constant was estimated, and the sample thermally annealed at 500 °C was found to exhibit the highest activity. The strong correlation between the TiO₂ crystalline characteristics and photocatalytic performance suggests that the synergistic coupling of the anatase and brookite crystalline domains led to effective charge separation upon photoirradiation and hence improved photocatalytic activity, most probably as a consequence of the vectorial displacement at the nanoscale junctions between

these crystalline grains that impeded the dynamics of electron–hole recombination. These results demonstrate the significance of nanoscale engineering in the manipulation of oxide photocatalytic performance.

Introduction

Photocatalysis of a chemical reaction at a semiconductor surface entails oxidation by the photogenerated holes and reduction by the photogenerated electrons that occur simultaneously [1]. Titania, a kind of semiconductor materials with very low cost, chemical inertness and photostability [2–4], has attracted extensive attention as one of the most promising materials in solar cells and photocatalysis [5–7]. The earliest work of photocatalysis of titania was reported in 1921 by Renz [8], where it was found that titania turned from white to a dark color under sunlight illumination in the presence of an organic compound such as glycerol. Photocatalytic activity of TiO₂ was also demonstrated by Fujishima and Honda [9] where they used TiO₂ for water splitting, an important process for solar energy conversion. In addition, Frank and Bard [10, 11] showed that the photocatalytic activity of TiO₂ might be exploited for the decomposition of pollutants under photo irradiation. In these reactions, the fundamental mechanisms [12–14] entail the rapid excitation of TiO₂ valence electrons to the conduction band by absorbing photons with energy larger than the TiO₂ bandgap (~3.0 eV), where the photogenerated electrons (conduction band) and holes (valence band) are involved in varied redox reactions.

Nevertheless, the efficiency of TiO₂ photocatalysis is generally rather low. Therefore, substantial efforts have been devoted to engineering the TiO₂ crystalline and morphological structures for the improvement of the

X. Kang · S. Chen (✉)
Department of Chemistry and Biochemistry, University
of California, 1156 High Street, Santa Cruz, CA 95064, USA
e-mail: schen@chemistry.ucsc.edu

photocatalytic activity. One effective approach is to fabricate nanotubule arrays of TiO_2 by taking advantage of the high surface-to-volume ratio, the ready accessibility of the TiO_2 surface to reactants and easy release of photoreaction products. A number of synthetic protocols have been reported in the literature for the fabrication of TiO_2 nanotubes, including electrochemical anodic oxidation of titanium metal sheets [15], as well as template-based atomic layer deposition [16], sol–gel [17], or liquid phase deposition [18–21] method. Among these, Grimes and coworkers [15] reported an effective route in 2001 toward the fabrication of titania nanotube arrays by anodization of a titanium foil in fluoride-based electrolyte solutions by using fluoride ions as effective etchants. It has been found that the nanotube morphology [22], length and pore size [23], as well as wall thickness [24] might be readily controlled by varied experimental parameters such as electrolyte composition, solution pH, as well as electrode voltage [25].

Furthermore, postsynthesis thermal annealing offers a powerful route toward the manipulation of the TiO_2 crystalline characteristics, in particular, transformation from one crystalline phase to another as well as control of the size of the nanocrystalline grains [26]. Note that titania of both anatase and rutile crystalline phases has been found to be photocatalytically active, although it is generally accepted that anatase TiO_2 exhibits a better performance, largely because of the somewhat higher Fermi level and the lower recombination rate of its photogenerated electrons and holes than those of the rutile phase [27–30]. In addition, the coexistence of both anatase and brookite or rutile crystalline phases has also been found to lead to further improvement of the photocatalytic performance, as a consequence of the vectorial displacements at the nanoscale junctions between two semiconducting domains that further impede the dynamics of electron–hole recombination [31–37]. However, in these earlier studies, the TiO_2 samples with a mixture of the crystalline phases were mostly prepared by the sol–gel methods in the form of nanoparticles, powders, or thin films, and it has remained a challenge to identify optimal experimental conditions for the production of TiO_2 nanotubes with significant brookite contents.

In this study, we demonstrate for the first time that brookite crystalline characteristics may also be produced in anodized TiO_2 nanotube arrays by a deliberate manipulation of the thermal annealing conditions. The results show that upon thermal annealing at 400–600 °C, the nanotube arrays exhibited clear anatase crystalline characteristics, in comparison with the largely amorphous structure of the as-produced samples. More interestingly, at 470 °C a second phase of brookite crystalline features also started to appear, which became much better defined at 500 °C. At higher

temperatures (550–600 °C), the brookite phase disappeared and only the anatase phase was found within the TiO_2 nanotube arrays. Overall, the photocatalytic activity of these thermally annealed TiO_2 nanotube arrays, as manifested in the photoreduction of methylene blue, displayed a marked improvement as compared to that of the amorphous as-prepared sample, and reached the maximum with samples that were thermally annealed at 500 °C (with a binary mixture of anatase and brookite phases), suggesting the impacts of the synergistic interactions between the anatase and brookite crystalline domains on the photocatalytic activity. Such a strong correlation demonstrates the significance of nanoscale engineering in the manipulation and optimization of the TiO_2 structures, properties and functions.

Experimental section

Methylene blue (ACROS), ethylene glycol (99+%, Aldrich) and ammonium fluoride (NH_4F , 98+%, extra pure, ACROS) were used without further treatment. Titanium foils (0.25 mm thick, 99.8% purity (metal basis)) were purchased from Aldrich. Before the experiments, the titanium sheets were degreased by sonication in acetone, ethanol, and Nanopure water successively and then dried in nitrogen. TiO_2 nanotube arrays were prepared by using a two-electrode setup in which a titanium foil was used as the sacrificial anode and a Pt wire as the cathode, along with an electrolyte consisting of 0.25% NH_4F in ethylene glycol. All the electrochemical reactions were carried out at room temperature by using a DC regulated power supply (B&K Precision Corp., Model 1623A) at the constant voltage of 60 V. The nanotube arrays were then subject to thermal annealing in air at varied temperatures in a muffle furnace for 6 h.

The structures of the TiO_2 nanotubes were then examined by SEM measurements with an ISI WB-6 scanning electron microscope operated at 5 kV. The crystalline characteristics were evaluated by powder X-ray diffraction (XRD) measurements, where the nanotubes were scratched off from the titanium metal sheets and deposited onto an Al plate, with a Rigaku Mini-flex Powder Diffractometer using $\text{Cu-K}\alpha$ radiation with a Ni filter ($\lambda = 0.154059$ nm at 30 kV and 15 mA). The average crystalline grain size was calculated from the XRD line broadening of the TiO_2 anatase (101) or brookite (121) diffraction peaks by using the Debye–Scherrer equation (in the calculations, the instrumental broadening was taken into account, which was calibrated with a standard Si sample [26, 38]).

The photocatalytic reduction of methylene blue by TiO_2 nanotubes was monitored spectrophotometrically with an ATI Unicam UV4 spectrometer by using a 1-cm quartz

cuvette with a resolution of 2 nm. Prior to exposure to UV lights, the TiO₂ nanotubes (1 cm × 1 cm) were immersed into the methylene blue solution (concentration 26 μM in water) for at least 40 min in the dark in a nitrogen atmosphere until no further decrease of the absorption intensity of methylene blue was observed. Optical absorption profiles were then acquired at different exposure times to the UV lights (365 nm, 6 W). Note that the solution was blanketed with a nitrogen atmosphere during the entire experimental procedure.

Results and discussion

The surface morphology of the TiO₂ nanotube arrays was first characterized by scanning electron microscopic (SEM) measurements. Figure 1 depicts two representative SEM micrographs of a TiO₂ nanotube array that was prepared at an anodic voltage of 60 V and then thermally annealed at 550 °C for 6 h. From the top view (panel a), one can see that a very dense array of rather uniform tubule structures was formed, with a tube density of ca. $7.4 \times 10^{11} \text{ cm}^{-2}$, and the inner diameter of the tube was found to be around 100 nm, and tube thickness ca. 35 nm. From the side view (panel b), the nanotube exterior surface was rather smooth and the length was about 10 μm.

Whereas variation of the thermal annealing temperature did not lead to obvious differences in terms of nanotube dimensions and surface morphologies, the crystalline details of the nanotube arrays were found to vary substantially, as manifested in powder X-ray diffraction (XRD) measurements. Figure 2 shows the XRD patterns of the TiO₂ nanotube arrays thermally annealed at different temperatures from 400 to 600 °C, along with that of the as-produced sample. In comparison to the standard XRD profiles for anatase, brookite, and rutile TiO₂, it can be seen that the as-prepared sample exhibited only a featureless profile (curve a), suggesting that the nanotubes were mostly amorphous (the several sharp features marked with “A1” arose from the aluminum substrate). In contrast, thermal annealing at elevated temperatures led to effective transformation of the nanotubes into well-defined crystalline structures. Specifically, for the nanotube arrays that were thermally annealed at 400–430 °C (curves b and c), a series of diffraction peaks appeared (marked with “@”), which are all consistent with the diffraction features of anatase TiO₂ (JCPDS 75-1537): (101), 25.7°; (200), 47.9°; (105), 53.7°; (211), 55.0°; (213), 61.9°; (204), 62.8°; (116), 68.3°; (220), 69.7°; and (301), 75.2°. When the annealing temperature was increased to 470 °C (curve d), in addition to the anatase diffraction features, several diffraction peaks characteristic of the brookite phase also started to appear, and they became much better defined at 500 °C (curve e),

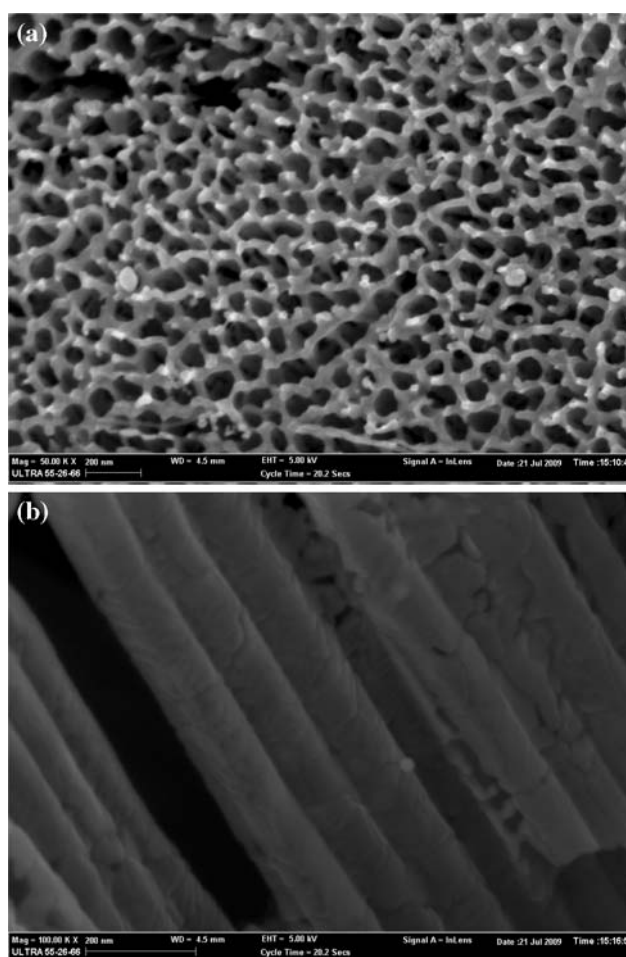
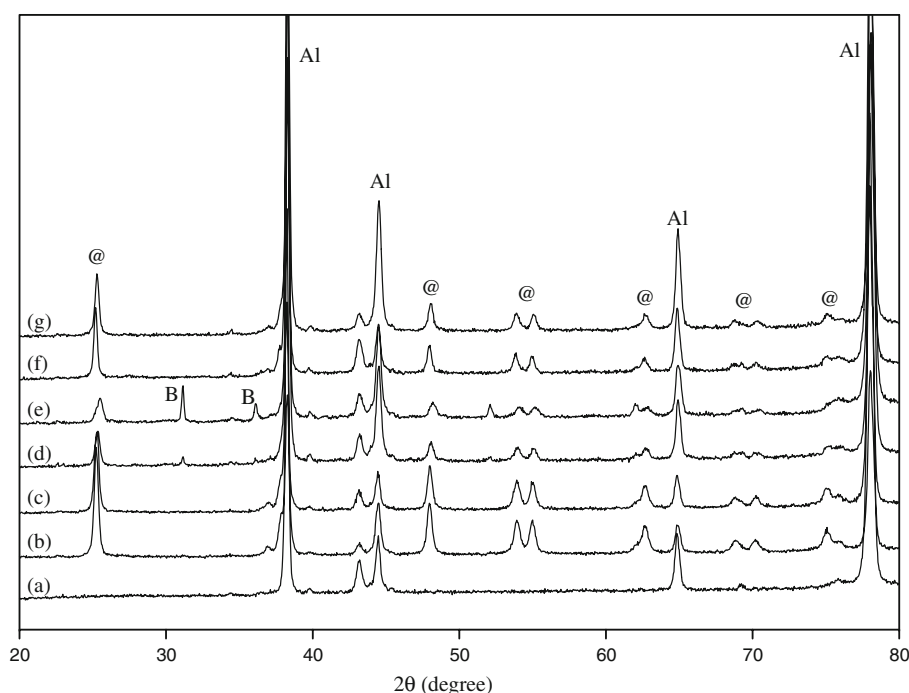


Fig. 1 Representative SEM micrographs of TiO₂ nanotube arrays that were prepared by electroanodization at 60 V followed by thermal annealing at 550 °C for 6 h. Scale bars are 200 nm in both **a** top view and **b** side view

as manifested by the peaks (marked with “B”) at 31.2° and 36.1°, which were ascribed to the brookite (121) and (012) crystalline lattices, respectively. In other words, within the narrow temperature range of 470 to 500 °C, the TiO₂ nanotube arrays exhibited a binary mixture of anatase and brookite crystalline phases. To the best of our knowledge, such an observation has not been reported previously with TiO₂ nanotubes prepared by electroanodization [25]. It should be noted that in most early studies where TiO₂ exhibited a mixture of crystalline phases, the titania samples were mostly thin films, powders, or nanoparticles that were prepared by sol–gel methods [31–37]. For instance, Junin et al. [33] prepared TiO₂ powders by a sol–gel method using titanium tetrachloride and titanium tetraisopropoxide as the precursors. A binary mixture of anatase and brookite crystalline phases was found at calcination temperatures between 400 and 500 °C.

Interestingly, with the further increase of the annealing temperature to 550 and 600 °C, the brookite diffraction

Fig. 2 XRD patterns of *a* the as-prepared TiO₂ nanotube arrays as well as those that underwent thermal annealing at different temperatures: *b* 400 °C, *c* 430 °C, *d* 470 °C, *e* 500 °C, *f* 550 °C, and *g* 600 °C. *Al* denotes diffraction features from the aluminum substrate, “@” refers to diffraction peaks of anatase TiO₂, whereas *B* marks those of brookite TiO₂



features disappeared and the sample again exhibited a pure anatase phase, suggesting the back conversion of brookite into anatase rather than further transformation into rutile. This indicates that for the TiO₂ nanotube arrays prepared above, the transformation between anatase and brookite was reversible at temperatures up to 600 °C, possibly because of the low activation energy (11.9 kJ/mol [26]) for the transformation between these two phases.

The grain size of the crystalline domains in the TiO₂ nanotubes was then evaluated quantitatively by the Debye–Scherrer equation, $D = K\lambda/\beta\cos\theta$, where D is the diameter of the crystalline grain, $K = 0.9$, $\lambda(\text{Cu-K}\alpha) = 1.54059 \text{ \AA}$, and β is the full width at half maximum of the selected diffraction peaks. Based on the anatase (101) diffraction peaks, the average size of the anatase crystalline domains at different annealing temperature was then estimated and listed in Table 1. It can be seen that the variation of the anatase grain size with annealing temperature is relatively small from 400 to 600 °C. For instance, the anatase grains decreased somewhat from 27.4 nm at 400 °C to 21.3 nm at 500 °C, possibly because of the formation of the brookite

crystalline domains that occurred at 470–500 °C (based on the brookite (121) diffraction peak, the brookite grains were estimated to be about 53.8 nm at 470 °C and 46.2 nm at 500 °C). At temperatures higher than 500 °C, the brookite phase disappeared, and the anatase crystalline grains became slightly larger to 29.6 nm at 550 °C and 25.7 nm at 600 °C [39]. The small anatase crystalline grains (Table 1) might also explain why no rutile feature was observed even at 600 °C, as the critical size for the transformation into rutile has been found to be >35 nm [26].

The effects of the evolution of the anatase nanocrystalline grains on the nanotube photocatalytic activity were then examined by using the reduction of methylene blue as the illustrating example. As methylene blue absorbs very strongly in the visible range with two well-defined absorption peaks at 612 and 665 nm and the reduced form is colorless, the photocatalytic reduction of methylene blue by TiO₂ may then be monitored by the spectrophotometric method. Mechanistically, it is generally proposed that upon UV illumination, electrons are excited from the TiO₂ valence band to the conduction band. The photogenerated electrons may then be exploited for reduction of methylene blue. As oxygen is an effective electron scavenger, it is important that the reaction media is protected with an inert atmosphere of nitrogen. Figure 3a depicts the optical absorption profiles of methylene blue after the solution was exposed to UV photoirradiation for varied periods of time in the presence of a TiO₂ nanotube array that was annealed at 500 °C for 6 h. It can be seen that the absorption features diminish rather quickly upon UV photoirradiation,

Table 1 Average grain size of the anatase (D_A) and brookite (D_B) phases in TiO₂ nanotube arrays that were thermally annealed at different temperatures (T)

T (°C)	400	430	470	500	550	600
D_A (nm) ^a	27.4	22.2	25.0	21.3	29.6	25.7
D_B (nm) ^b			53.8	46.2		

^a Based on anatase (101) diffraction peak

^b Based on brookite (121) diffraction peak

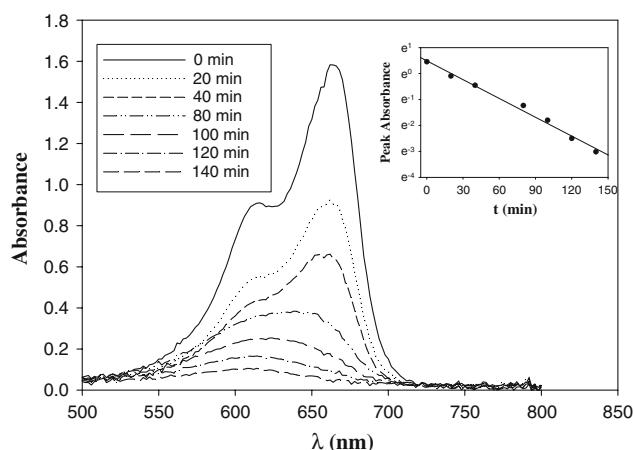


Fig. 3 Visible absorption profiles of a methylene blue solution (26 μM in water) after being exposed to UV photoirradiation for varied periods of time (shown as figure legends) in the presence of a TiO_2 nanotube array that was thermally annealed at 500 $^{\circ}\text{C}$ for 6 h. *Inset* depicts the semilog plot of the variation of the intensity of the absorption peak at 665 nm with UV exposure time. *Symbols* are experimental data and *line* is linear regression

suggesting the effective photocatalytic activity of TiO_2 in the reduction of methylene blue. Panel (b) shows the semilog plots of the decay of the absorption intensity at 665 nm with time. The linearity is consistent with the first-order reaction of methylene blue reduction [40], and from linear regression the pseudo-first-order rate constant was estimated to be $2.42 \times 10^{-2} \text{ min}^{-1}$.

The photocatalytic activity of the TiO_2 nanotubes annealed at other temperatures was evaluated in a similar fashion. Figure 4a depicts the decay profiles of methylene blue absorption at 665 nm with TiO_2 nanotubes that were thermally annealed at different temperatures, along with that of the as-prepared nanotubes. It can be seen that all annealed samples exhibited apparent enhancement of the photocatalytic activity in the reduction of methylene blue as compared to the as-prepared sample. In addition, among the series, the diminishment of the methylene blue absorption feature was the fastest for the sample annealed at 500 $^{\circ}\text{C}$. Panel (b) shows the pseudo-first-order rate constants (k) that were estimated from linear regressions of the dynamics curves in panel (a). It can be seen that for the as-prepared sample, k is $2.30 \times 10^{-3} \text{ min}^{-1}$. It increased markedly to $1.00 \times 10^{-2} \text{ min}^{-1}$ and $1.24 \times 10^{-2} \text{ min}^{-1}$ with TiO_2 nanotubes thermally annealed at 400 and 430 $^{\circ}\text{C}$, respectively. At higher temperatures, the rate constant increased further to $1.70 \times 10^{-2} \text{ min}^{-1}$ at 470 $^{\circ}\text{C}$ and $2.42 \times 10^{-2} \text{ min}^{-1}$ at 500 $^{\circ}\text{C}$. Further increase of the thermal annealing temperature actually saw a decrease of the reaction rate constant to $9.69 \times 10^{-3} \text{ min}^{-1}$ at 550 $^{\circ}\text{C}$ and 1.02×10^{-2} at 600 $^{\circ}\text{C}$. That is, the maximal photocatalytic performance was observed with TiO_2 nanotubes annealed at

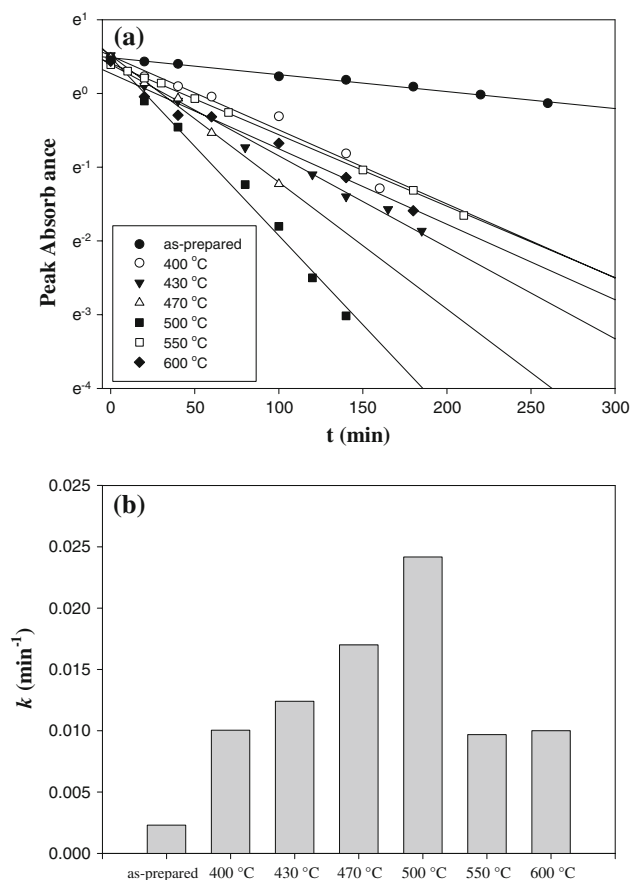


Fig. 4 **a** Semilog plots of the variation of the intensity of the absorption peak at 665 nm with UV exposure time for the photocatalytic reduction of methylene blue by TiO_2 nanotubes that were thermally annealed at different temperatures (shown as figure legends). The experimental conditions were the same as those in Fig. 3. *Symbols* were experimental data and *lines* were linear regressions, from which the pseudo-first-order reaction rate constants (k) were evaluated, as depicted in panel (**b**)

500 $^{\circ}\text{C}$, which coincided with the formation of a binary mixture of anatase and brookite nanocrystalline domains [41, 42], as manifested in Fig. 2. This is most probably because of the vectorial displacements of the photogenerated electrons at nanoscale junctions between these two semiconducting phases that retard the charge recombination process and hence enhance the charge separation efficiency [43, 44]. In fact, enhanced photocatalytic performance of TiO_2 with a binary mixture of anatase and brookite crystalline phases, as compared to that of pure anatase, has been reported in a number of studies [44–47].

Nevertheless, one might also argue that the variation of the photocatalytic performance is a consequence of the effective oxide surface area that reaches the maximum at 500 $^{\circ}\text{C}$. However, this is unlikely because an increase of calcination temperature typically leads to a monotonic decrease of the TiO_2 surface area [33]. Additionally, on

the basis of Raman spectroscopic measurements (not shown), the impact of TiO₂ surface functionalities on the photocatalytic activity appears to be minimal, as no apparent difference of the Raman spectra was observed among the nanotube arrays thermally annealed at different temperatures (400–600 °C) [48].

Conclusion

TiO₂ nanotube arrays were prepared by anodization of Ti metal sheets and characterized by SEM and XRD measurements. SEM study showed that the nanotubes formed a rather dense array, and XRD measurements indicated that whereas the as-prepared samples were largely amorphous, thermal annealing at elevated temperatures (400–600 °C) led to the effective formation of crystalline nanotubes with clear anatase features. Interestingly, at 470 °C, a second crystalline phase of brookite features also started to emerge, which became better defined at 500 °C. The presence of a binary mixture of anatase and brookite crystalline phases within this narrow range of annealing temperature was found to coincide with the maximal photocatalytic activity of the TiO₂ nanotubes in the reduction of methylene blue. This is accounted for by the vectorial displacements of the photogenerated electrons at nanoscale junctions between these two semiconducting phases that retard the charge recombination process and hence enhance the charge separation efficiency. This study demonstrates the fundamental significance of nanoscale engineering in the manipulation of the properties and functions of nanoscale materials.

Acknowledgements This work was supported in part by the National Science Foundation (DMR-0804049) and ACS-PRF (49137-ND10).

Open Access This article is distributed under the terms of the Creative Commons Attribution Noncommercial License which permits any noncommercial use, distribution, and reproduction in any medium, provided the original author(s) and source are credited.

References

- Fujishima A, Zhang XT, Tryk DA (2008) *Surf Sci Rep* 63:515
- Serpone N, Pelizzetti E (1989) *Photocatalysis: fundamentals and applications*. Wiley, New York
- Schiavello M (1985) *Photoelectrochemistry, photocatalysis, and photoreactors: fundamentals and developments*. D. Reidel Pub. Co.; Sold and distributed in the USA and Canada by Kluwer Academic, Dordrecht
- Linsebigler AL, Lu GQ, Yates JT (1995) *Chem Rev* 95:735
- Bozzi A, Yuranova T, Kiwi J (2005) *J Photochem Photobiol* 172:27
- Bozzi A, Yuranova T, Guasaquillo I, Laub D, Kiwi J (2005) *J Photochem Photobiol* 174:156
- Ferguson MA, Hoffmann MR, Hering JG (2005) *Environ Sci Technol* 39:1880
- Renz C (1921) *Helvet Chim Acta* 4:961
- Fujishima A, Honda K (1972) *Nature* 238:37
- Frank SN, Bard AJ (1977) *J Am Chem Soc* 99:303
- Frank SN, Bard AJ (1977) *J Phys Chem* 81:1484
- Goodeve CF, Kitchener JA (1938) *Trans Faraday Soc* 34:570
- Goodeve CF, Kitchener JA (1938) *Trans Faraday Soc* 34:902
- Kennedy DR, Ritchie M, Mackenzie J (1958) *Trans Faraday Soc* 54:119
- Gong D, Grimes CA, Varghese OK, Hu WC, Singh RS, Chen Z, Dickey EC (2001) *J Mater Res* 16:3331
- Sander MS, Cote MJ, Gu W, Kile BM, Tripp CP (2004) *Adv Mater* 16:2052
- Maiyalagan T, Viswanathan B, Varadaraju UV (2006) *Bull Mater Sci* 29:705
- Cochran RE, Shyue JJ, Padture NP (2007) *Acta Mater* 55:3007
- Yamanaka S, Hamaguchi T, Muta H, Kurosaki K, Uno M (2004) *J Alloys Compd* 373:312
- Hsu MC, Leu IC, Sun YM, Hon MH (2005) *J Cryst Growth* 285:642
- Hamaguchi T, Uno M, Yamanaka S (2005) *J Photochem Photobiol* 173:99
- Mor GK, Varghese OK, Paulose M, Mukherjee N, Grimes CA (2003) *J Mater Res* 18:2588
- Cai QY, Paulose M, Varghese OK, Grimes CA (2005) *J Mater Res* 20:230
- Mor GK, Shankar K, Paulose M, Varghese OK, Grimes CA (2005) *Nano Lett* 5:191
- Paulose M, Shankar K, Yoriya S, Prakasham HE, Varghese OK, Mor GK, Latempa TA, Fitzgerald A, Grimes CA (2006) *J Phys Chem B* 110:16179
- Zhang HZ, Banfield JF (2000) *J Phys Chem B* 104:3481
- McIntock IS, Ritchie M (1965) *Trans Faraday Soc* 61:1007
- Fox MA, Dulay MT (1993) *Chem Rev* 93:341
- Brown JD, Williamson DL, Nozik AJ (1985) *J Phys Chem* 89:3076
- Maruska HP, Ghosh AK (1978) *Sol Energy* 20:443
- Zheng RB, Meng XW, Tang FQ (2009) *Appl Surf Sci* 255:5989
- Hao HY, Zhang JL (2009) *Mater Lett* 63:106
- Junin C, Thanachayanont C, Euvananont C, Inpor K, Limthongkul P (2008) *Eur J Inorg Chem* 974
- Tian GH, Fu HG, Jing LQ, Xin BF, Pan K (2008) *J Phys Chem C* 112:3083
- Tseng YH, Kuo CS, Huang CH, Li YY, Chou PW, Cheng CL, Wong MS (2006) *Nanotechnology* 17:2490
- Hou XH, Choy KL (2005) *Mater Sci Eng C* 25:669
- Watson S, Beydoun D, Scott J, Amal R (2004) *J Nanopart Res* 6:193
- Chen W, Ghosh D, Chen SW (2008) *J Mater Sci* 43:5291. doi: [10.1007/s10853-008-2792-x](https://doi.org/10.1007/s10853-008-2792-x)
- Mor GK, Varghese OK, Paulose M, Shankar K, Grimes CA (2006) *Sol Energy Mater Sol Cells* 90:2011
- Wu XM, Ling YH, Liu L, Huang ZH (2009) *J Electrochem Soc* 156:K65
- Di Paola A, Cufalo G, Addamo M, Ellardita MB, Campostrini R, Ischia M, Ceccato R, Palmisano L (2008) *Colloids Surf A* 317:366
- Zhao B, Chen F, Huang QW, Zhang JL (2009) *Chem Commun* 5115
- Yan MC, Chen F, Zhang JL, Anpo M (2005) *J Phys Chem B* 109:8673
- Ozawa T, Iwasaki M, Tada H, Akita T, Tanaka K, Ito S (2005) *J Colloid Interf Sci* 281:510

45. Ardizzone S, Bianchi CL, Cappelletti G, Gialanella S, Pirola C, Ragaini V (2007) *J Phys Chem C* 111:13222
46. Yu JC, Yu JG, Zhang LZ, Ho WK (2002) *J Photochem Photobiol A* 148:263
47. Yu JG, Yu JC, Leung MKP, Ho WK, Cheng B, Zhao XJ, Zhao JC (2003) *J Catal* 217:69
48. Zhang YH, Chan CK, Porter JF, Guo W (1998) *J Mater Res* 13:2602